Carbon isotope minima in the South Atlantic during the last deglaciation: evaluating the influence of air-sea gas exchange

Environmental Research Letters

LETTER

Carbon isotope minima in the South Atlantic during the last deglaciation: evaluating the influence of air-sea gas exchange

D Lund[1], J Hertzberg[2] and M Lacerra[3]

[1] Department of Marine Sciences, University of Connecticut, United States of America
[2] Department of Ocean, Earth, and Marine Sciences, Old Dominion University, United States of America
[3] Department of Geosciences, Princeton University, United States of America

E-mail: david.lund@uconn.edu

Keywords: carbon isotopes, deglaciation, air-sea gas exchange, Atlantic meridional overturning circulation

Supplementary material for this article is available online

OPEN ACCESS

RECEIVED
29 November 2018

REVISED
28 February 2019

ACCEPTED FOR PUBLICATION
22 March 2019

PUBLISHED
3 May 2019

Abstract

Carbon isotope minima were a ubiquitous feature in the mid-depth (1.5–2.5 km) Atlantic during Heinrich Stadial 1 (HS1, 14.5–17.5 kyr BP) and the Younger Dryas (YD, 11.6–12.9 kyr BP), with the most likely driver being collapse of the Atlantic Meridional Overturning Circulation (AMOC). Negative carbon isotope anomalies also occurred throughout the surface ocean and atmosphere, but their timing relative to AMOC collapse and the underlying drivers have remained unclear. Here we evaluate the lead-lag relationship between AMOC variability and surface ocean $\delta^{13}C$ signals using high resolution benthic and planktonic stable isotope records from two Brazil Margin cores (located at 1.8 km and 2.1 km water depth). In each case, the decrease in benthic $\delta^{13}C$ during HS1 leads planktonic $\delta^{13}C$ by 800 $\pm$ 200 years. Because the records are based on the same samples, the relative timing is constrained by the core stratigraphy. Our results imply that AMOC collapse initiates a chain of events that propagates through the oceanic carbon cycle in less than 1 kyr. Direct comparison of planktonic foraminiferal and atmospheric records implies a portion of the surface ocean $\delta^{13}C$ signal can be explained by temperature-dependent equilibration with a ^{13}C-depleted atmosphere, with the remainder due to biological productivity, input of carbon from the abyss, or reduced air-sea equilibration.

1. Introduction

The rise in atmospheric CO_2 during the last deglaciation was first documented over 30 years ago (Neftel *et al* 1982) yet the underlying mechanisms responsible for the signal remain unclear (Broecker 1982, Sigman *et al* 2010). The initial rise in CO_2 during Heinrich Stadial 1 (HS1) coincided with a decrease in the $\delta^{13}C$ of CO_2 (Schmitt *et al* 2012), implying the carbon originated from a ^{13}C-depleted reservoir. The atmospheric $\delta^{13}C$ record is remarkably similar to $\delta^{13}C$ time series from the mid-depth Atlantic, implying both reflect the input of isotopically light carbon from a common source (figure 1). While the mid-depth signal is likely due to collapse of the AMOC (Lund *et al* 2015, Oppo *et al* 2015), the atmospheric signal may be due to upwelling of light carbon in the Southern Ocean (Spero and Lea 2002, Menviel *et al* 2018), weakening of the biological pump (Menviel *et al* 2015, Schmittner and Lund 2015), or some combination of these effects (Bauska *et al* 2016). In this paper, we review evidence for collapse of the AMOC during HS1, focusing on results from the Brazil Margin, a location with a well-developed depth transect of cores that can be used to monitor the relative timing of circulation and carbon cycle changes in the surface, mid-depth (1.5–2.5 km) and abyssal Atlantic. We focus on two Brazil Margin cores, including KNR159-5-78GGC (27.5°S, 46.3°W, 1800 m) and KNR159-5-33GGC (27.6°S, 46.2°W, 2100 m). Using benthic and planktonic $\delta^{13}C$ records from these cores we evaluate the relative timing of AMOC collapse and changes in the oceanic carbon cycle. We also estimate the predicted changes in surface ocean $\delta^{13}C$ at the Brazil Margin using available atmospheric $\delta^{13}C$ records and a new planktonic foraminiferal Mg/Ca time series from core KNR159-5-78GGC. We

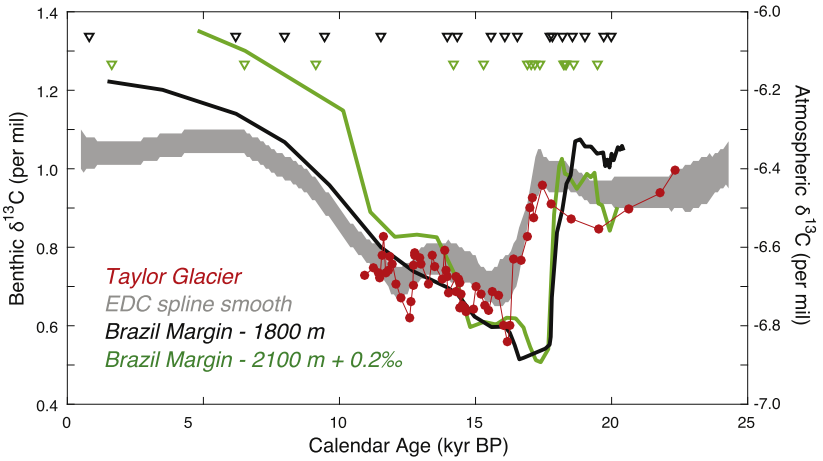

Figure 1. Mid-depth Brazil Margin $\delta^{13}C$ time series compared to atmospheric $\delta^{13}C$ of CO_2 from 0–25 kyr BP. The benthic foraminiferal records are simple three-point running mean values of *C. wuellerstorfi* $\delta^{13}C$ for 1800 m (black line) and 2100 m water depth (green line) (Tessin and Lund 2013). Note that the results at 2100 m are shifted by +0.2‰. Triangles denote calendar ages for each Brazil Margin record, assuming a regional reservoir age (ΔR) of 0 ± 200 years (1σ). Both time series indicate $\delta^{13}C$ decreased abruptly at 17.8 kyr BP. Two records of atmospheric $\delta^{13}C$ are shown, including the spline smooth of Epica Dome C (EDC) data (gray area; Schmitt *et al* 2012) and the discrete estimates from the Taylor Glacier record (red circles; Bauska *et al* 2016). The gray zone for EDC represents the ±1σ uncertainty around the mean value (see Schmitt *et al* 2012 for details). The shift in atmospheric $\delta^{13}C$ during HS1 occurs 300–400 years earlier when either the AICC2012 age model (Veres *et al* 2012) or (Parrenin *et al* 2013) age model is applied to the EDC record.

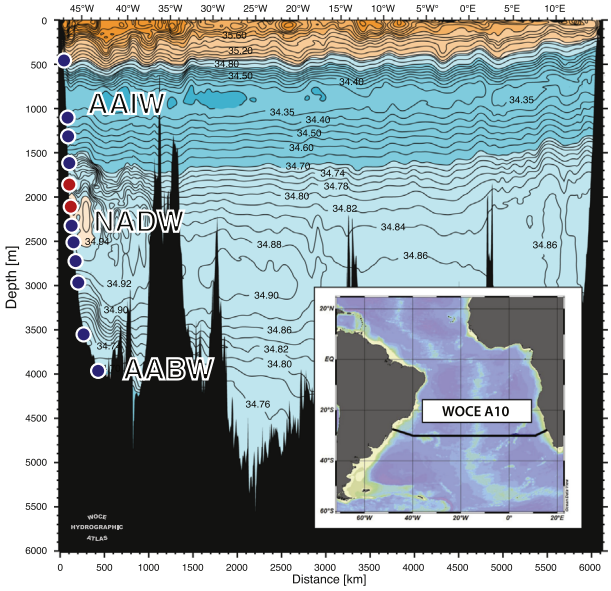

Figure 2. Brazil Margin core locations superimposed on the WOCE A10 salinity section (https://doi.org/10.21976/CGRP4Z). Symbols represent cores with radiocarbon-constrained time series summarized in Lund *et al* (2015). Red symbols mark the depths of the two cores that are the focus of this study (KNR159-5-78GGC at 1800 m and KNR159-5-33GGC at 2100 m). Also noted are the approximate depths of Antarctic Intermediate Water (AAIW), North Atlantic Deep Water (NADW), and Antarctic Bottom Water (AABW).

then compare the predicted and observed $\delta^{13}C$ records to assess the drivers of surface ocean $\delta^{13}C$ variability during millennial-scale events of the last deglaciation.

1.1. Hydrographic context

The Brazil Margin depth transect is located on the western edge of the South Atlantic subtropical gyre (figure 2). At the latitude of the core sites (~27°S), near surface waters are influenced by the Brazil Current (BC), which is composed of warm, saline Tropical Water in the upper 150 m (Tsuchiya *et al* 1994) and cooler, fresher South Atlantic Central Water (SACW) from ~150 to 800 m (Tomczak and Godfrey 1994). The BC originates from the southern South Equatorial Current, which approaches South America from the east and bifurcates at ~15°S (Peterson and Stramma 1991), with approximately 8 Sv flowing northward, eventually becoming the North Brazil Current, and 4 Sv flowing southward as the weaker BC (Stramma *et al* 1990). Recirculating flow within the gyre causes BC transport to increase to ~10 Sv

by 27°S (Peterson and Stramma 1991). Surface-mixed layer records based on planktonic foraminifera such as *G. sacculifer* and *G. ruber* should therefore reflect hydrographic conditions in the BC and the broader South Atlantic subtropical gyre.

Near 40°S, the approximate latitude of the Subtropical Front, the BC encounters the northward flowing Malvinas Current before combining and flowing offshore as the South Atlantic Current, which bounds the southern edge of the gyre (Peterson and Stramma 1991). Wintertime convection in the Brazil-Malvinas confluence region creates a range of Subtropical Mode Waters that are found from ~150 to 400 m water depth at the Brazil Margin (i.e. the shallow portion of SACW) (Gordon 1981, Provost *et al* 1999). At 27°S, the hydrographic properties of the upper thermocline are set by the lightest of these mode waters, which originate in the confluence region from ~32°S to 40°S in the Southwest Atlantic (Provost *et al* 1999). Further south, between the Subtropical Front and Sub-Antarctic Front, the formation of Sub-Antarctic Mode Water contributes to the deeper portion of SACW (~400 to 800 m water depth) (Stramma and England 1999). Thus, records based on thermocline dwelling foraminifera such as *N. dutertrei* should reflect the influence of not only the BC, but also the Malvinas Current, which originates in the Southern Ocean.

Deeper in the water column, the Brazil Margin sites are influenced by North Atlantic Deep Water (NADW) and Antarctic Bottom Water (AABW) (figure 2). NADW is clearly outlined by the maximum in salinity centered at ~2500 m, which is apparent in vertical profiles from the Holocene as a maximum in $\delta^{13}C$ and minimum in $\delta^{18}O$ (Hoffman and Lund 2012) (figure S1 is available online at stacks.iop.org/ERL/14/055004/mmedia). The Brazil Margin transect also monitors low salinity AABW as it enters the abyssal South Atlantic (figure 2), which is reflected in the $\delta^{13}C$ minimum and $\delta^{18}O$ maximum in the deepest portion of the Holocene profiles (figure S1). Core-top $\delta^{13}C$ results for the deepest sites average 0.4% (Hoffman and Lund 2012), indistinguishable from the value for AABW (Kroopnick 1985). Core-top $\delta^{18}O$ results for the deepest sites (3.2% $\pm$ 0.2%) are also similar to estimates of AABW $\delta^{18}O$ based on modern hydrographic data (~3.1%) (Hoffman and Lund 2012).

1.2. Background

As described in detail in the supplemental materials, the mid-depth Brazil Margin sites were strongly influenced by Glacial North Atlantic Intermediate Water (GNAIW) during the LGM. At 1800 m, the watermass mixture was approximately 75% GNAIW and 25% GAABW (figure 3(a)), while at 2100 m, the proportions were ~60% and 40%, respectively (Tessin and Lund 2013). During HS1, the $\delta^{18}O$ and $\delta^{13}C$ at each site decreased by approximately 0.5% (figure 3(b)). In contrast, deeper sites showed little or no change (Lund *et al* 2015). The overall HS1 pattern at the Brazil Margin is therefore one of large signals at mid-depth and little or no variability below 2500 m. The trajectory of the mid-depth Brazil Margin anomalies parallels the trend in northern component water (NCW), indicating the sites responded to the shift in NCW composition. Modeling simulations and carbonate ion reconstructions suggest the Brazil Margin $\delta^{13}C$ anomalies were due to collapse of the AMOC and accumulation of respired carbon at mid-depth (Schmittner and Lund 2015, Lacerra *et al* 2017), while the $\delta^{18}O$ anomalies were likely due to input of isotopically light melt water and subsurface warming (Zhang *et al* 2017). Modeled collapse of the AMOC also yields negative $\delta^{13}C$ anomalies in the surface ocean due to reduced biological export of light carbon and air-sea gas exchange with a ^{13}C-depleted atmosphere (Schmittner and Lund 2015). The Brazil Margin and atmospheric $\delta^{13}C$ time series in figure 1 may therefore reflect distinct biogeochemical consequences of AMOC collapse, with the former reflecting accumulation of respired carbon and the latter responding to exchange with a ^{13}C-depleted surface ocean.

If AMOC collapse triggered the surface ocean and atmosphere response, then proxies of the AMOC should lead proxies of surface ocean carbon cycle change during HS1. Model simulations suggest the time lag is approximately 1 kyr, due to propagation of the signal via the deep ocean circulation (Schmittner and Lund 2015). While declining $\delta^{13}C$ at the Brazil Margin appears to lead atmospheric $\delta^{13}C$ (figure 1), uncertainty in the age models for both sediment and ice cores precludes a clear determination of the lead-lag relationship (Tessin and Lund 2013). Here we address this problem by evaluating the relative timing of benthic and planktonic $\delta^{13}C$ anomalies in the same sediment cores. We use mid-depth sites from the Brazil Margin, where benthic $\delta^{13}C$ should reflect AMOC variability and planktonic $\delta^{13}C$ should reflect equilibration with a ^{13}C-depleted atmosphere. Using atmospheric $\delta^{13}C$ and planktonic foraminiferal Mg/Ca records, we assess whether temperature mediated air-sea gas exchange on its own can explain the surface mixed layer and thermocline-depth $\delta^{13}C$ records. We also address the recent suggestion by Lynch-Stieglitz *et al* (2019) that the mid-depth anomalies could be due to temperature-mediated air-sea gas exchange.

2. Methods

The $\delta^{13}C$ of planktonic foraminifera reflects not only the $\delta^{13}C$ of dissolved inorganic carbon (DIC) but also respiration, photosynthetic fractionation by algal symbionts, seawater carbonate ion concentration, and vertical migration (Curry and Crowley 1987, Spero and Lea 1993, 1996, Spero *et al* 1997, Spero *et al* 2003). Many of these vital effects influence the carbon

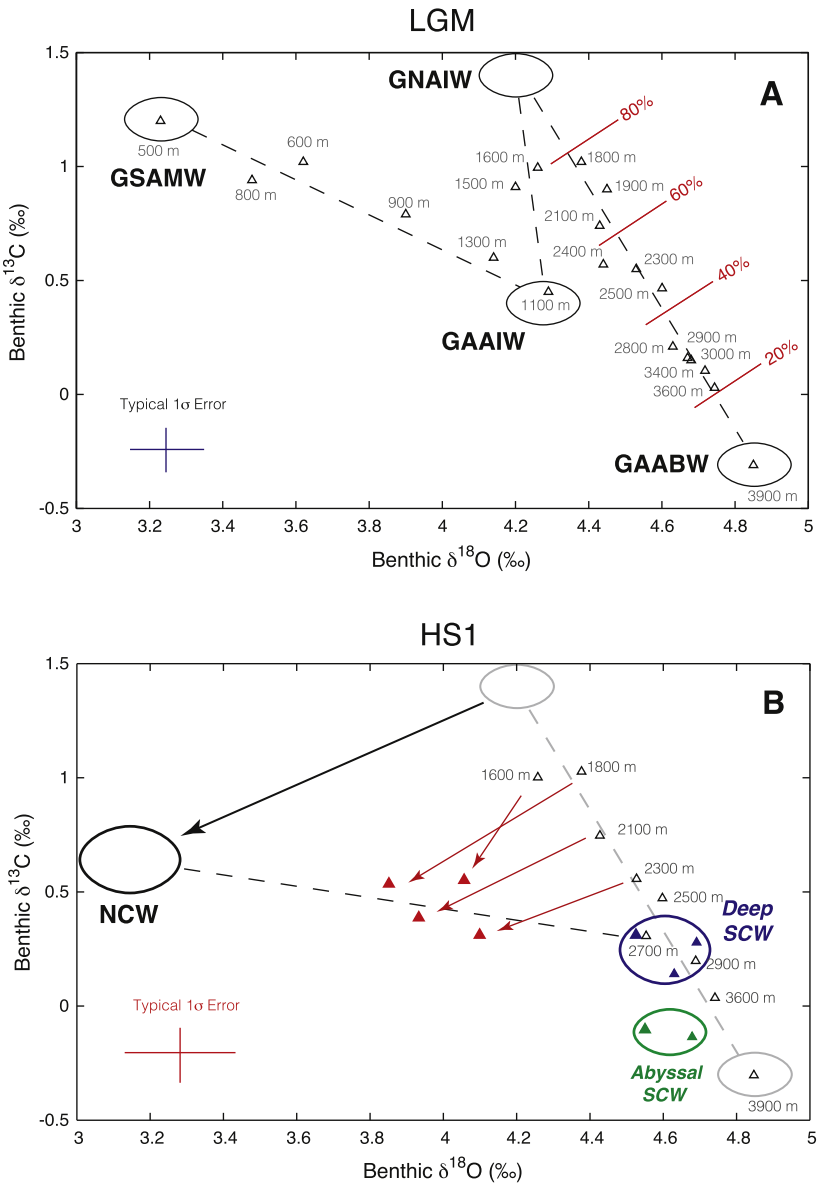

Figure 3. Cross-plots of $\delta^{13}C$ versus $\delta^{18}O$ for the Brazil Margin. (A) LGM cross-plot, including data from Curry and Oppo (2005) above 3100 m water depth and Hoffman and Lund (2012) below 3100 m (see figure S1). The SW Atlantic was occupied by four distinct water masses during the LGM, including Glacial Antarctic Bottom Water (GAABW), Glacial North Atlantic Intermediate Water (GNAIW), Glacial Antarctic Intermediate Water (GAAIW) and Glacial Sub-Antarctic Mode Water (GSAMW). At depths ranging from 1700 to 3900 m, the isotopic values reflect a two-component mixture of GNAIW and GAABW. Red percentages indicate the proportion of GNAIW. (B) HS1 cross-plot, including Brazil Margin data from 1600 to 2500 m (Tessin and Lund 2013), 2700 to 3000 m (Lund *et al* 2015), and 3600 to 3900 m (Hoffman and Lund 2012). The HS1 results are grouped into three isotopically distinct watermasses, including mid-depth water (red triangles), deep southern component water (SCW) (blue triangles), and abyssal southern component water (green triangles). Also shown is the estimated $\delta^{13}C$ and $\delta^{18}O$ range for northern component water (NCW) during HS1 (see Lund *et al* 2015 for details). The mid-depth results plot on the mixing line between NCW and deep SCW.

isotopic composition in the surrounding micro-environment, which is the source of calcifying fluid for the shell (Zeebe *et al* 1999). One way to control for vital effects is to use multiple planktonic species, including those with and without symbionts and those that dwell at surface and thermocline depths. Given that many vital effects are size-dependent, it is also important to use shells from as narrow a size range as possible. To characterize the surface mixed-layer, we use *G. sacculifer* (300–355 μm size fraction), focusing on individuals without the sac-like terminal chamber (Curry and Crowley 1987, Spero *et al* 2003). We also use the *N. dutertrei* data from Hertzberg *et al* (2016) to characterize the upper thermocline (Fairbanks *et al* 1982, Curry and Crowley 1987, Multiza *et al* 1999). Following Spero *et al* (2003), Hertzberg *et al* (2016) employed *N. dutertrei* individuals from the >350 μm size fraction that lacked evidence for secondary crusting. Note that the *G. sacculifer* record is from core 33GGC while the *N. dutertrei* record is from core 78GGC.

To minimize sampling uncertainty in the stable isotope time series, we crushed and homogenized 20–40 *G. sacculifer* tests from each sample and then ran four

separate aliquots of powder to determine the mean $\delta^{13}C$ for each stratigraphic level. This approach was necessary to extract the cleanest possible $\delta^{13}C$ signal for comparison to the benthic $\delta^{13}C$ time series in 33GGC. Given their larger size relative to *G. sacculifer* and therefore greater CO_2 yield, Hertzberg *et al* (2016) crushed and homogenized 4–8 *N. dutertrei* tests from each sample and then ran four separate aliquots of powder to determine the mean $\delta^{13}C$ at each stratigraphic level. The analyses for both species were run on a Finnigan MAT 253 triple-collector gas source mass spectrometer coupled to a Finnigan Kiel automated carbonate device at the University of Michigan's Stable Isotope Laboratory. Isotope values were corrected to VPDB using National Bureau of Standards 19 ($n = 53$, $\delta^{13}C = 1.92\% \pm 0.05\%$, $\delta^{18}O = -2.18\% \pm$ 0.05%). The benthic stable isotope records used to assess the relative timing of mid-depth and surface ocean $\delta^{13}C$ anomalies were originally presented in Tessin and Lund (2013). We use the calendar-calibrated age models for 33GGC and 78GGC from Lund *et al* (2015), which are updated versions of those originally presented in Tessin and Lund (2013).

In order to assess the influence of sea surface temperature (SST) on $\delta^{13}C$, a new *G. ruber* Mg/Ca time series was generated for core 78GGC. We picked ~40 shells from each sample (250–355 μm size fraction, average total weight ~580 μg). The shells were gently crushed between glass plates, homogenized, and split into two aliquots for replicate analyses. Each sample underwent a cleaning procedure that included clay removal, metal oxide reduction, and organic matter oxidation (Boyle and Keigwin 1985, Rosenthal *et al* 1997). All samples were dissolved in 2% HNO_3 and run on a Thermo Element 2 ICP-MS at UCONN Avery Point. Samples were corrected for drift using a 2% HNO_3 blank and 100 ppm Ca standard (Mg/Ca = 3.40 mmol mol^{-1}). Analytical precision (1σ), determined using two external standards with Mg/Ca ratios of 3.20 and 3.60 mmol mol^{-1}, was 0.50% ($n = 12$) and 0.38% ($n = 12$), respectively. In addition, Al/Ca, Mn/Ca, and Fe/Ca ratios were measured to monitor for clays and metal oxides not removed during the cleaning procedure. Mg/Ca ratios were converted to SST using the species-specific *G. ruber* calibration equation of Anand *et al* (2003). This calibration yields an average late-Holocene SST of 23.2 °C, similar to modern average annual SST at the core site of 23.6 °C (Locarnini *et al* 2013).

3. Results and discussion

3.1. Planktonic foraminiferal stable isotope records

Both *G. sacculifer* and *N. dutertrei* $\delta^{18}O$ decreased by ~1.5% during the deglaciation, with an initial decline during HS1, a pause during the B-A, and then a second decline during the YD (figure 4). There is a brief increase in $\delta^{18}O$ at ~5 kyr BP in the *G. sacculifer* record but it is unclear whether a similar feature exists in the *N. dutertrei* time series because of its lower resolution during the Holocene. In general, the two $\delta^{18}O$ records maintain a 0.3%–0.5% offset from 0 to 20 kyr BP, with the exception of the B-A and early YD where the $\delta^{18}O$ values converge (figure 4(c)). If the 0.3%–0.5% $\delta^{18}O$ difference is entirely due to temperature, it would imply that *G. sacculifer* calcified in 1 °C–2 °C warmer water, consistent with its shallower habitat.

The $\delta^{13}C$ time series also show broadly similar patterns during the deglaciation, including negative carbon isotope anomalies during HS1 and the YD (figure 4). The *N. dutertrei* HS1 anomaly, defined here as the $\delta^{13}C$ difference between the 15–16 kyr BP and 18–20 kyr BP time intervals, is $-0.66\% \pm 0.07\%$. The uncertainty is based on the standard error of the mean values for time window. By comparison, the YD anomaly, defined as the difference between 11–12 kyr BP and 13–14 kyr BP, is $-0.32\% \pm 0.17\%$. Thus, the $\delta^{13}C$ signal is greater during HS1 than the YD. In the case of *G. sacculifer*, the HS1 anomaly is $-0.49 \pm 0.08\%$, while the YD anomaly is $-0.34\% \pm 0.10\%$. Here the HS1 signal also appears to be larger but the uncertainties preclude a clear statement on their relative magnitude. Overall the two records display remarkably similar millennial-scale variability (figure 4(f)). Given that *G. sacculifer* dwells in the surface mixed layer, while *N. dutertrei* calcifies in the upper thermocline, our results suggest the $\delta^{13}C$ of DIC declined during both HS1 and the YD. The *G. sacculifer* record also shows a negative excursion at ~8 kyr BP (figure 4(e)) that is not resolved by the *N. dutertrei* time series (figure 4(d)).

3.2. Relative timing of benthic, planktonic, and atmospheric signals

The negative shifts in *N. dutertrei* and *G. sacculifer* $\delta^{13}C$ during HS1 lag the respective benthic $\delta^{13}C$ time series in each core (figure 5). The inset in each panel of figure 5 shows the correlation versus lag relationship for the planktonic and benthic $\delta^{13}C$ records for the 20 to 15 kyr BP interval (i.e. the LGM to HS1). Positive values indicate planktonic $\delta^{13}C$ lags benthic $\delta^{13}C$. In core 78GGC, the maximum correlation ($r^2 = 0.89$) occurs at a lag of 800 ± 100 years, which is nearly constant during the LGM to HS1 transition. In core 33GGC, the maximum correlation ($r^2 = 0.88$) is similar but spans a wider range (800 ± 300 years). The broader time span is due a smaller lag near the beginning of HS1 which steadily increases until ~16 kyr BP. Overall, however, the planktonic records lag their benthic counterparts by approximately 800 years. While the absolute age of the $\delta^{13}C$ anomalies may change with future age model updates, the relative timing of the benthic and planktonic records is set by the core stratigraphy. In each core, the decline in benthic $\delta^{13}C$ occurs 10–20 cm prior the decline in planktonic $\delta^{13}C$, larger than can be explained by bioturbation. Furthermore, planktonic and benthic

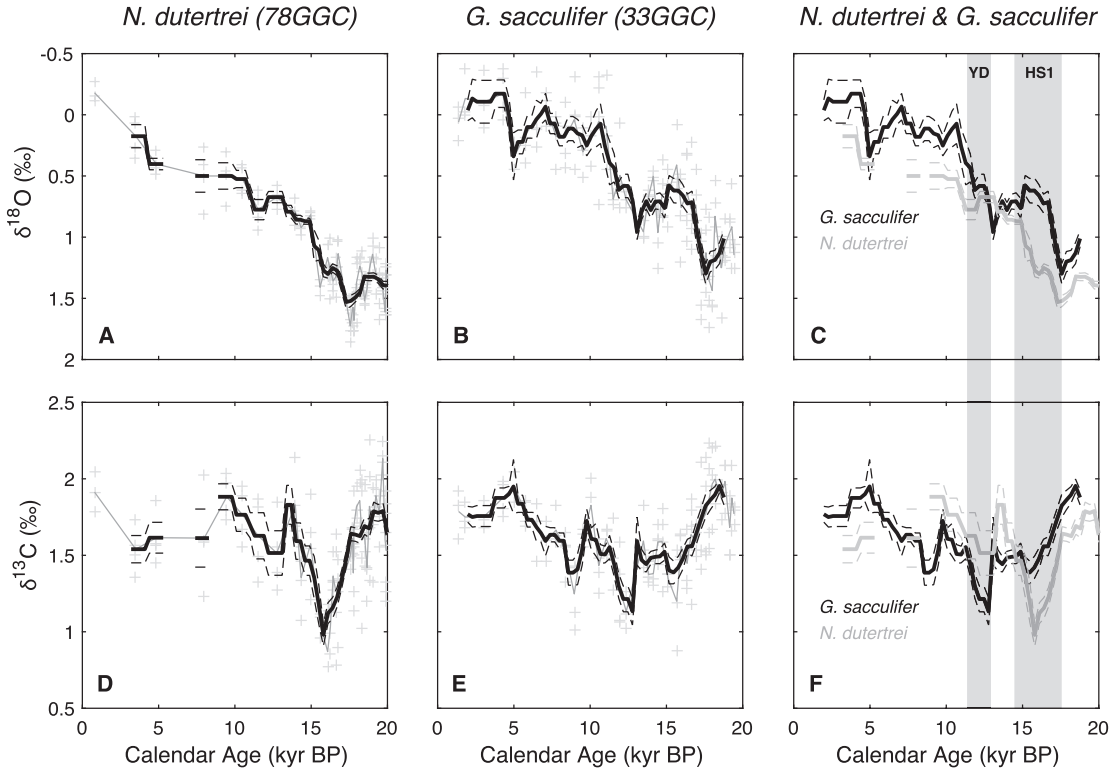

Figure 4. Planktonic stable isotope records from KNR159-5-78GGC (*N. dutertrei*) and KNR159-5-33GGC (*G. sacculifer*). (A) *N. dutertrei* δ^{18}O results, including discrete analyses (+), the average at each stratigraphic level (thin gray line), the 1 kyr running mean (thick black line), and the standard error for the running mean (dashed lines). (B) Same as panel A but for *G. sacculifer*. (C) Running mean values for *G. sacculifer* (black) and *N. dutertrei* (gray). (D)–(F) Same as panels (A)–(C) but for δ^{13}C. Vertical gray bars mark the approximate time intervals for HS1 (14.5–17.5 kyr BP) and the YD (11.6–12.9 kyr BP).

shells used in our analyses are from a similar size fraction (>250 μm), so preferential sorting based on shell size is unlikely.

The lag between benthic and planktonic δ^{13}C is similar to the observed lag between benthic and atmospheric δ^{13}C in figure 1. Here, however, atmospheric δ^{13}C appears to lag benthic δ^{13}C not only during HS1 but also later in the deglaciation (8–12 kyr BP). To quantify this difference, we linearly detrended each record and determined the correlation coefficient between the resulting time series at a range of lags spanning 0 to 3000 years (figure 6). Positive values indicate atmospheric δ^{13}C lags benthic δ^{13}C. To assess the sensitivity of our results to the choice of atmospheric record, we used EDC (Schmitt *et al* 2012), EDC on the timescale of Veres *et al* (2012), and the Taylor Glacier δ^{13}C results (Bauska *et al* 2016). For core 78GGC, we find that the maximum correlation with atmospheric δ^{13}C occurs at lags of 900–1300 years. Similarly, the maximum correlation for core 33GGC occurs at lags of 800–1200 years. For both cores, the smallest lag (800–900 years) occurs using the Veres *et al* (2012) timescale for EDC. The largest lags occur using the Schmitt *et al* (2012) timescale for EDC (1200–1300 years), while the Taylor Glacier results have intermediate values (1000–1100 years). On average, atmospheric δ^{13}C lags benthic δ^{13}C by ~1000 years, similar to the 800 year offset between benthic and planktonic δ^{13}C (figure 5).

The generally greater lag for the atmospheric records is likely due to uncertainty in the ice core and sediment core age models. One possibility is that reservoir ages at the Brazil Margin were higher during the deglaciation (e.g. 600 years versus 400 years), which would bring the lag estimates in figure 6 into agreement with the benthic-planktonic offset. Alternatively, the Veres *et al* (2012) timescale for EDC, which is similar to that of Parrenin *et al* (2013), may be the most accurate age model for atmospheric δ^{13}C. If this is the case, then the benthic-atmosphere lag (800–900 years) would overlap the benthic-planktonic offset. Regardless of the details, it is clear that atmospheric and surface ocean δ^{13}C lagged the mid-depth signal, which is inconsistent with the idea that air-sea equilibration drove δ^{13}C variability throughout the upper Atlantic (Lynch-Stieglitz *et al* 2019). Instead, our results are consistent with AMOC collapse causing the accumulation of respired carbon at mid-depths (Lacerra *et al* 2017), with a subsequent carbon cycle response in the surface ocean.

3.3. Inferred sea-surface temperatures

The SST time series for core 78GGC shows the anticipated glacial to interglacial pattern, with a total

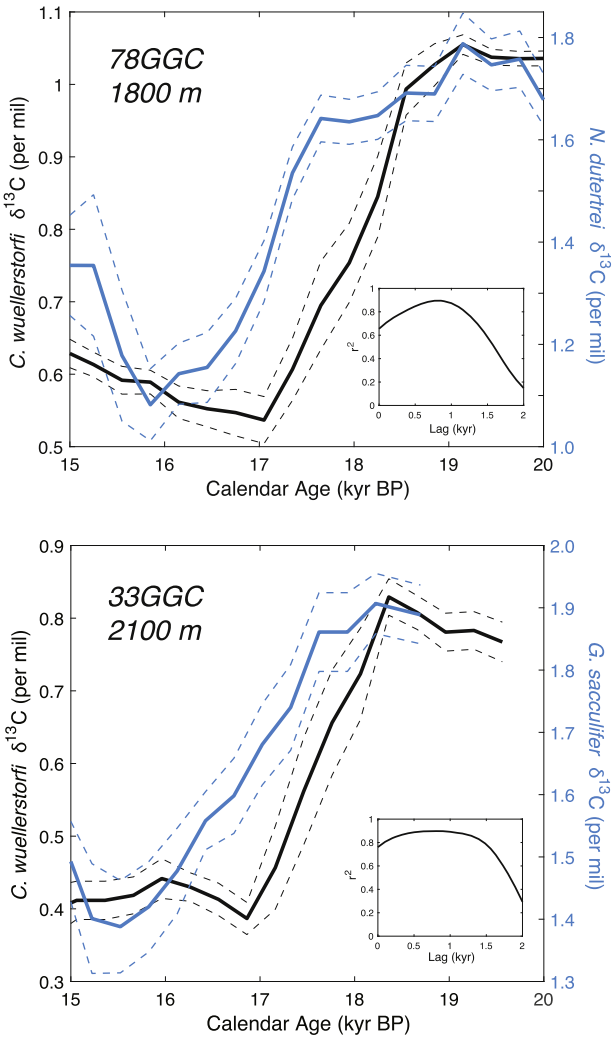

Figure 5. Surface and mid-depth Brazil Margin $\delta^{13}C$ records for the 15–20 kyr BP time interval, including 1 kyr running mean values (solid lines) and standard error on the running mean (dashed lines). (Top) Planktonic (*N. dutertrei*) and benthic (*C. wuellerstorfi*) $\delta^{13}C$ records from KNR159-5-78GGC (1800 m water depth). Inset depicts correlation versus lag relationship for the two records; positive lag values indicate planktonic $\delta^{13}C$ lags benthic $\delta^{13}C$. (Bottom) Planktonic (*G. sacculifer*) and benthic (*C. wuellerstorfi*) $\delta^{13}C$ records from KNR159-5-33GGC (2100 m water depth). Inset depicts correlation versus lag relationship for the two records. In each case, the decline in benthic $\delta^{13}C$ precedes planktonic $\delta^{13}C$ by ~800 years.

LGM to Holocene SST increase of ~2 °C (figure 7(a)). The SST rise occurs late in the deglaciation, however, with nearly all of the signal occurring from 15 to 13 kyr BP (i.e. the Bølling-Allerød or B-A). After 12 kyr BP, SSTs remained persistently high, with values ranging from 23.5 to 24.5 °C. SSTs peaked at ~6 kyr BP, followed by a cooling of 0.5 °C–1.0 °C during the late Holocene. The SST pattern in 78GGC is similar to that reconstructed by Carlson *et al* (2008) using *G. ruber* Mg/Ca from core KNR159-5-36GGC (figure 7(b)). Thus, two Brazil Margin Mg/Ca time series show that deglacial warming in the surface mixed layer occurred during the B-A, indicating that the *G. sacculifer* $\delta^{18}O$ signal during HS1 was likely due to changes in $\delta^{18}O_{sw}$. The Mg/Ca results also imply that the negative anomaly in *G. sacculifer* $\delta^{13}C$ during HS1 was due to factors other than SST, with the caveat that the long equilibration time for $\delta^{13}C$ means that it likely reflects the integrated temperature history of subtropical gyre surface waters at the Brazil Margin. The relevance of the *G. ruber* Mg/Ca results for *N. dutertrei* $\delta^{13}C$ are less clear given their different depth habitats. However, the small $\delta^{18}O$ offset between *G. sacculifer* and *N. dutertrei* $\delta^{18}O$ during the deglaciation (<0.5%) implies they experienced a similar temperature history. During the first half of HS1, when *N. dutertrei* $\delta^{13}C$ decreased by 0.6%, the corresponding decrease in $\delta^{18}O$ was relatively modest (~0.2%; figure 4(c)), equivalent to a maximum warming of 1 °C.

3.4. The effect of air-sea gas exchange on planktonic $\delta^{13}C$

Given the similar lag between: (1) benthic and planktonic $\delta^{13}C$, and (2) benthic $\delta^{13}C$ and atmospheric $\delta^{13}C$, the relative timing between the planktonic and atmospheric $\delta^{13}C$ records is likely correct to within several hundred years. The records can therefore be directly compared to assess the influence of air-sea gas exchange on planktonic

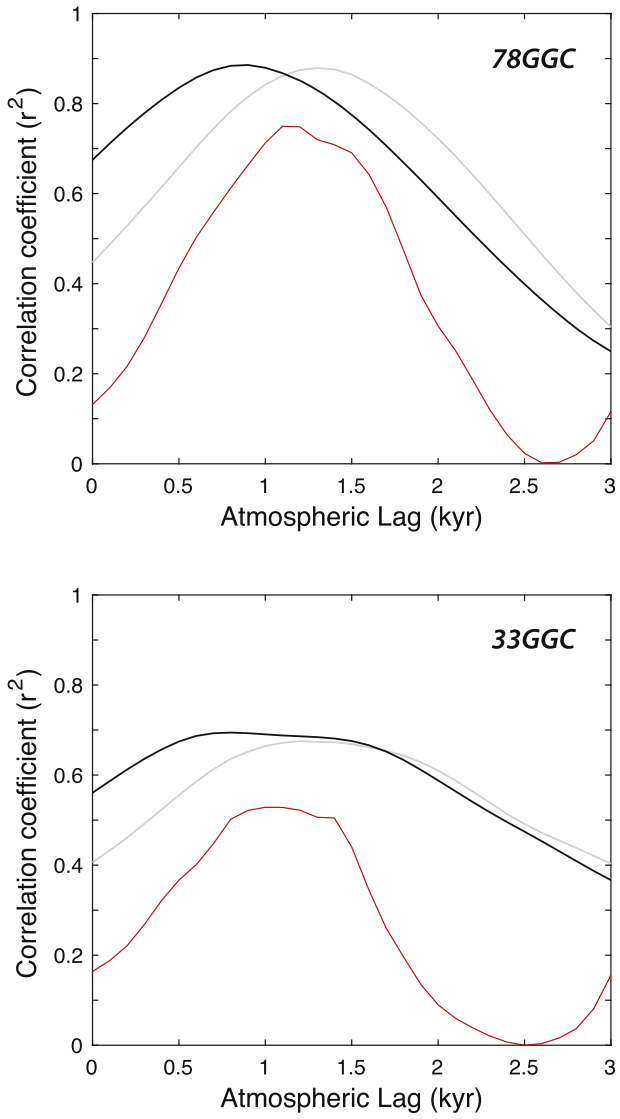

Figure 6. Correlation versus lag relationships for the Brazil Margin benthic δ^{13}C records relative to atmospheric δ^{13}C. (Top) Results for KNR159-5-78GGC versus atmospheric δ^{13}C, including EDC on the timescale of Schmitt *et al* (2012) (gray line), EDC on the timescale of Veres *et al* (2012) (black line), and Taylor Glacier (Bauska *et al* 2016) (red line). The maximum correlation occurs when atmospheric δ^{13}C lags benthic δ^{13}C by 900–1300 years. The Veres *et al* (2012) age scale yields the smallest lag (~900 years). (Bottom) Same as top panel, but for KNR159-5-33GGC. The maximum correlation occurs when atmospheric δ^{13}C lags benthic δ^{13}C by 800–1200 years. The Veres *et al* (2012) age scale yields the smallest lag (~800 years).

δ^{13}C. Overall, the atmospheric and oceanic data display similar millennial-scale variability; in each case, δ^{13}C declined during HS1, increased during the B-A, decreased again during the YD, and finally rebounded to LGM-like values during the early Holocene (figure 8). While the timing is similar across records, the magnitude of the planktonic anomalies during HS1 and the YD (0.4%–0.6%) is approximately twice the atmospheric signal (0.2%–0.3%). (Note the *y*-axes in each panel of figure 8 are scaled so that the relative magnitude of the δ^{13}C signals is preserved.)

Surface ocean $\delta^{13}C_{DIC}$ can be influenced by a range of factors, including air-sea gas exchange, biological export of carbon from the surface ocean, and mixing with watermasses of different δ^{13}C composition. For the LGM, we can estimate how changes in atmospheric δ^{13}C and equilibration temperatures might impact surface water $\delta^{13}C_{DIC}$ at the Brazil Margin using ice core-derived atmospheric δ^{13}C data and SSTs inferred from planktonic foraminiferal Mg/Ca. This approach assumes that the SST signal at our site is broadly representative of locations in the subtropical gyre where surface water exchanges carbon with the atmosphere. At isotopic equilibrium, the fractionation between seawater DIC and gaseous CO_2 at 22 °C is approximately 8.2% (Zhang *et al* 1995). Assuming an atmospheric δ^{13}C of −6.4%, the expected δ^{13}C of DIC ($\delta^{13}C_{DIC}$) would be 1.8%, which falls within ±0.1% of the mean *G. sacculifer* and *N. dutertrei* values for the 18–20 kyr BP interval (figure 8(b)). This result is surprising considering the observed δ^{13}C offsets between foraminifera and DIC; the δ^{13}C of *N. dutertrei* is enriched relative to $\delta^{13}C_{DIC}$ by ~0.5% (Mulitza *et al* 1999) while the δ^{13}C of *G. sacculifer* (250–355 μm) has been

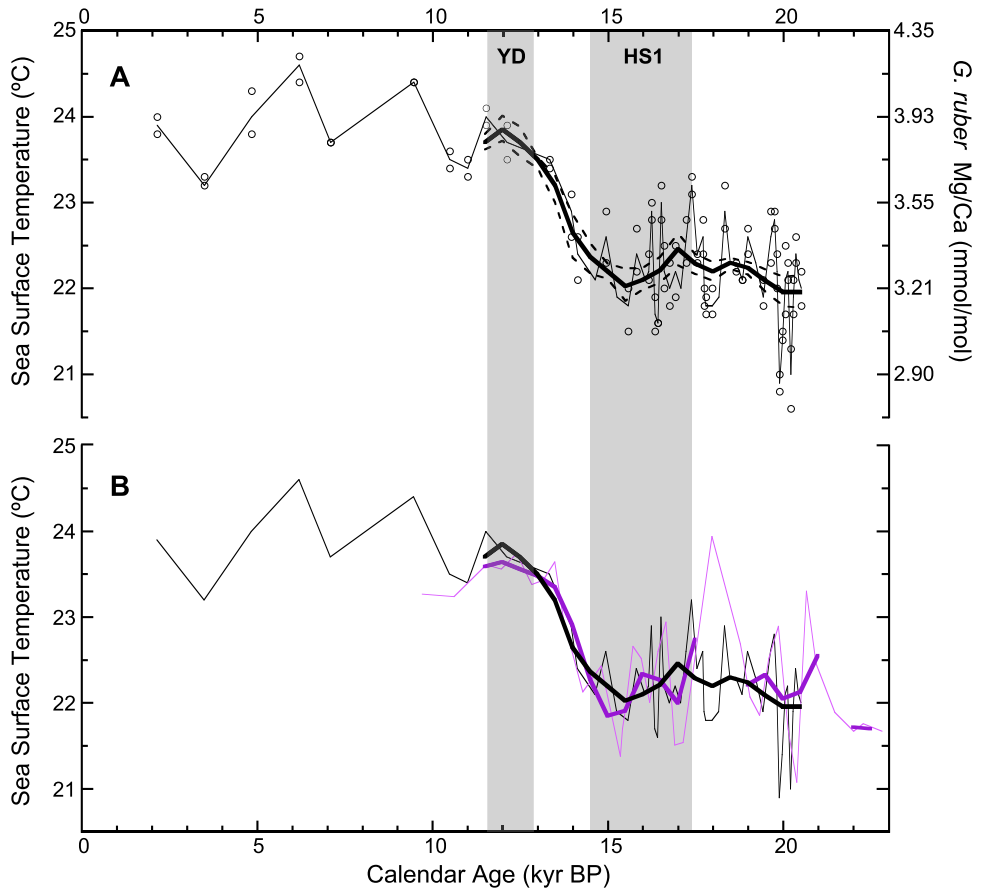

Figure 7. Sea-surface temperatures based on *G. ruber* Mg/Ca ratios from the Brazil Margin. (A) *G. ruber* Mg/Ca ratios (right *y*-axis) and calibrated SSTs (left *y*-axis) for core KNR159-5-78GGC. Circles are individual data points at each stratigraphic level and thin black line connects the average of these analyses. Intervals with only one point indicate there were only enough foraminifera for one analysis. The 1 kyr running mean (bold solid line) and standard error (dashed lines) are shown for the interval from 10 to 20 kyr BP. (B) Calibrated SSTs based on *G. ruber* Mg/Ca from core KNR159-5-78GGC (thin black line) and KNR159-5-36GGC (thin purple line, Carlson *et al* 2008). The 1 kyr running mean for 78GGC (bold black line) and 36GGC (bold purple line) are also shown.

shown to be depleted relative to $\delta^{13}C_{DIC}$ by ~0.1% (Spero *et al* 2003). Thus, the inferred $\delta^{13}C_{DIC}$ for the upper thermocline would be 0.5% less than the *N. dutertrei* $\delta^{13}C$ record, making it more depleted than the surface mixed layer $\delta^{13}C_{DIC}$ (based on *G. sacculifer*). Relatively depleted $\delta^{13}C$ values for the upper thermocline compared to the surface mixed layer are consistent with the observed upper ocean gradient in $\delta^{13}C_{DIC}$ driven by photosynthesis and respiration of organic matter (Kroopnick 1985, Mulitza *et al* 1999).

To determine the drivers of millennial-scale $\delta^{13}C$ variability at the Brazil Margin, we separately consider the influence of SST and atmospheric $\delta^{13}C$. In the first case, we assume atmospheric $\delta^{13}C$ was constant during last deglaciation and equal to the LGM value (−6.4%) but take into account temperature-dependent fractionation between DIC in seawater and CO_2 in air (Zhang *et al* 1995). The resulting $\delta^{13}C_{DIC}$ time series (dashed black line in figure 8(b)) shows no signal until the B-A, when $\delta^{13}C$ declines by approximately 0.2% due to the 2 °C increase in SST (figure 7). While the temperature-only $\delta^{13}C_{DIC}$ estimate shows lower values during the YD, similar to the planktonic $\delta^{13}C$ data, the lack of signal during HS1 indicates additional factors were responsible for the HS1 signal.

We consider the combined influence of atmospheric $\delta^{13}C$ and SST variability using the EDC record and assuming temperature-dependent ^{13}C equilibration. The resulting $\delta^{13}C_{DIC}$ time series, depicted as the solid red line in figure 8(b), shows a ~0.3% decline during HS1, followed by an additional ~0.2% drop during the YD. Here the predicted HS1 signal is due to exchange with an isotopically lighter atmosphere while the YD signal is due to both the atmospheric influence and warmer SSTs. A similar pattern occurs if we use the Taylor Glacier $\delta^{13}C$ record rather than EDC (dashed red line in figure 8(b)). Both of the predicted time series are similar to the *G. sacculifer* record; $\delta^{13}C$ declines during HS1, levels out during the B-A, and then declines again during the YD, reaching values lower than at any point during the deglaciation. The overall agreement suggests that temperature-dependent gas exchange with a ^{13}C-depleted atmosphere can account for the broad features of the *G. sacculifer* record. However, *G. sacculifer* shows a larger than predicted signal during HS1, which is most easily observed in the difference between

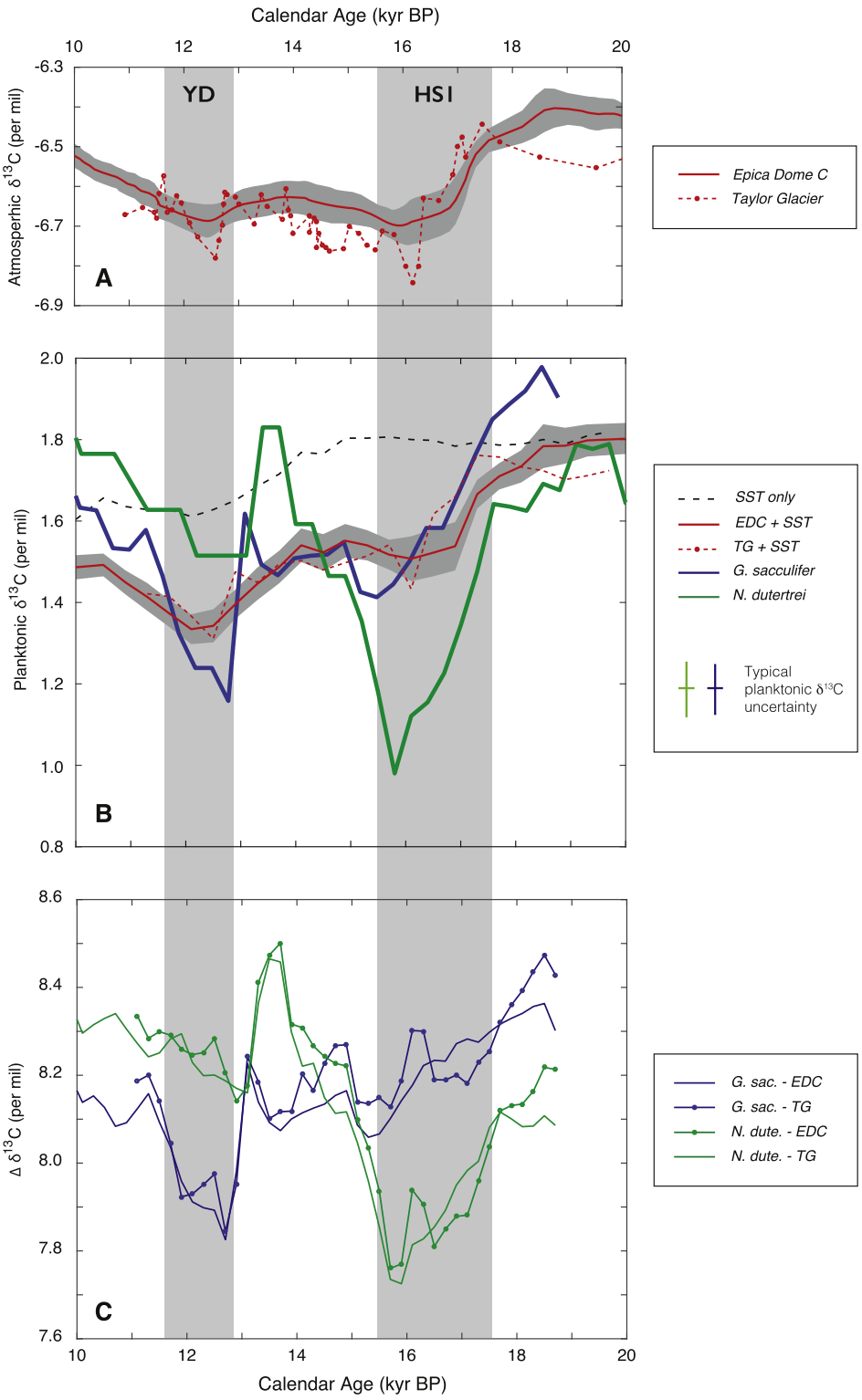

Figure 8. Atmospheric $\delta^{13}C$, Brazil Margin planktonic foraminiferal $\delta^{13}C$, and their difference ($\Delta\delta^{13}C$) during the last deglaciation. (A) Two records of atmospheric $\delta^{13}C$, including Taylor Glacier (red circles) (Bauska *et al* 2016) and the spline smooth of Epica Dome C (EDC) data on the timescale of Veres *et al* (2012) (red line). (B) Running mean planktonic stable isotope records for *G. sacculifer* (blue line), *N. dutertrei* (green line) (see figure 4 for detailed records). The thin dashed black line depicts the anticipated surface ocean $\delta^{13}C$ assuming atmospheric $\delta^{13}C = -6.4\%$ and the temperature-dependent ^{13}C fractionation between DIC in seawater and CO_2 in air (Zhang *et al* 1995), using the Mg/Ca-based SST record in figure 7. The red line with gray error envelope shows the anticipated surface ocean $\delta^{13}C$ based on the combined effect of variable atmospheric $\delta^{13}C$ (EDC record in top panel) and SST. The dashed red line is the same but for the Taylor Glacier $\delta^{13}C$ record. Note that no corrections have been applied to the planktonic $\delta^{13}C$ records. (C) The difference between atmospheric and planktonic $\delta^{13}C$ ($\Delta\delta^{13}C$), including *G. sacculifer* and EDC (blue line), *G. sacculifer* and Taylor Glacier (blue circles), *N. dutertrei* and EDC (green line), and *N. dutertrei* and Taylor Glacier (green circles).

atmospheric $\delta^{13}C$ and *G. sacculifer* $\delta^{13}C$ ($\Delta\delta^{13}C$) (blue lines in figure 8(c)). The *G. sacculifer* $\Delta\delta^{13}C$ values based on both EDC and Taylor Glacier decreased by 0.2%–0.3% during HS1. The *G. sacculifer* $\delta^{13}C$ anomaly is therefore 0.2%–0.3% greater than can be accounted for by equilibrium exchange with the atmosphere. During the YD, $\Delta\delta^{13}C$ also decreased 0.2%–0.3%, but about half of this signal can be attributed to warmer SSTs. The largest mismatch between the predicted and observed *G. sacculifer* $\delta^{13}C$ signals occurs during HS1.

In the case of *N. dutertrei*, the HS1 $\delta^{13}C$ anomaly is ~0.4% larger than can be accounted for by simple ocean-atmosphere equilibration (figure 8(c)). While it possible that temperatures warmed in the upper thermocline, the $\delta^{18}O$ data for *N. dutertrei* show only a modest decrease during HS1 (0.2%), equivalent to a maximum warming of ~1 °C. During the YD, the *N. dutertrei* $\delta^{13}C$ signal (0.3%) is closer the predicted anomaly due to SST warming (0.2%), suggesting that the combined effect of variable atmospheric $\delta^{13}C$ and SST can account for the majority of the *N. dutertrei* response at this time. Therefore, most of the YD signal for *G. sacculifer* and *N. dutertrei* can be explained by air-sea gas exchange but both species display a larger than expected $\delta^{13}C$ signal during HS1, particularly *N. dutertrei.* Given that atmospheric CO_2 increased during HS1, this would likely yield lower surface ocean $[CO_3^{2-}]$ values. As a result, we would expect the carbonate ion effect on planktonic $\delta^{13}C$, which has a slope of ~−0.01% per μmol kg^{-1} (Spero *et al* 1997), would yield positive $\delta^{13}C$ anomalies. Thus, other factors need to be invoked to explain the HS1 $\delta^{13}C$ signals.

3.5. Additional drivers of surface ocean $\delta^{13}C$

What caused the planktonic $\delta^{13}C$ anomalies during HS1? One possibility is that the surface ocean was less equilibrated with the atmosphere, perhaps due to weaker winds or a reduced residence time for surface waters in the South Atlantic. This seems unlikely, however, as *G. sacculifer* reflects conditions in the Brazil Current and broader subtropical gyre while *N. dutertrei* should track ventilated thermocline conditions further south. Alternatively, isotopically light carbon upwelled in the Southern Ocean during HS1 (Ninnemann and Charles 1997, Spero and Lea 2002) could have been transmitted northward through mixing and ventilation in the Brazil-Malvinas Current confluence region and then carried to the Brazil Margin via upper thermocline waters. This scenario could explain the larger than expected *N. dutertrei* $\delta^{13}C$ signal, but it is unclear how it would yield an anomalous response in *G. sacculifer*. Recently published model results suggest that increasing Southern Hemisphere westerlies by 50% relative to the LGM and decreasing freshwater input into the Southern Ocean by 0.2 Sv can yield substantial surface ocean and atmospheric $\delta^{13}C$ anomalies at the Brazil Margin (Menviel *et al* 2018). However, warming in Antarctica and the Southern Ocean during HS1 (Monnin *et al* 2001, Pahnke *et al* 2003, Lamy *et al* 2007, Barker *et al* 2009) makes it unlikely that regional freshwater fluxes decreased early in the deglaciation. Further data and model inter-comparison studies are necessary to assess the role of freshwater forcing in the Southern Ocean and its role in driving release of isotopically light carbon from the abyss.

One other possible explanation of the larger than expected $\delta^{13}C$ anomalies at Brazil Margin is weakening of the biological pump. Paired high resolution planktonic and benthic $\delta^{13}C$ records from multiple intermediate depth sites indicate the upper ocean $\delta^{13}C$ gradient decreased during HS1 (Hertzberg *et al* 2016). These data are consistent with the accumulation of isotopically light carbon in the surface ocean and less remineralization at intermediate depths. In this scenario, it is possible that *N. dutertrei* responded to reduced productivity in the Southern Ocean, with the associated surface ocean $\delta^{13}C$ anomaly transmitted northward to the Brazil-Malvinas confluence region. Consistent with this idea, alkenone flux results from the Sub-Antarctic suggest export productivity declined early in the deglaciation, most likely due to reduced iron fertilization (Martínez-García *et al* 2014).

Weakening of the biological pump is unlikely to a have a direct impact on *G. sacculifer* $\delta^{13}C$ given that nutrients are completely utilized in subtropical gyre surface waters. The $\delta^{13}C_{DIC}$ of these waters, and therefore the $\delta^{13}C$ of *G. sacculifer*, is more likely to reflect the influence of atmospheric equilibration (Schmittner and Lund 2015). This makes the larger than expected $\delta^{13}C$ anomaly for *G. sacculifer* during HS1 more difficult to explain. One possibility is that the signal was transmitted by the Brazil Current from the equatorial Atlantic, where either reduced biological productivity or upwelling of ^{13}C-depleted mode waters (as implied by the *N. dutertrei* results) created negative carbon isotope anomalies. Consistent with this idea, modeling results suggest that weakening of the AMOC causes an overall reduction in export production in the South Atlantic and basin-wide depletion in surface ocean ^{13}C (Menviel *et al* 2015). Alternatively, warming in the equatorial Atlantic during HS1 (Arbuszewki *et al* 2013) may have contributed to lower surface ocean $\delta^{13}C_{DIC}$ in this region, which was then transmitted to the core sites by the Brazil Current. Testing of these hypotheses will require additional high-resolution planktonic $\delta^{13}C$, Mg/Ca, and productivity records from the tropical, subtropical, and sub-polar South Atlantic. For the time being, however, it appears that air-sea exchange on its own is unable to explain the full magnitude of planktonic $\delta^{13}C$ anomalies at the Brazil Margin.

4. Conclusions

The goal of this paper has been to: (1) constrain the timescale on which AMOC perturbations propagate through the oceanic carbon cycle, and (2) evaluate the role of air-sea exchange in driving surface ocean $\delta^{13}C$ variability during the last deglaciation. In the first case,

we compare benthic and planktonic foraminiferal $\delta^{13}C$ records from sediment cores that monitor NCW in the Southwest Atlantic. Our findings, which are based on two different cores and planktonic species, indicate that negative carbon isotope anomalies at mid-depth led those in the surface ocean by 800 ± 200 years. This lag reflects the propagation time of AMOC collapse through the oceanic carbon cycle and its eventual expression in the surface ocean and atmosphere. This result is important because it implies that weakening of the AMOC plays a central role in surface ocean carbon isotope minima during glacial terminations. The timescale of signal propagation will be useful for testing simulations of the AMOC influence on the ocean carbon cycle. Our results also suggest that air-sea gas exchange is an unlikely explanation both mid-depth and surface ocean $\delta^{13}C$ anomalies in the Atlantic (Lynch-Stieglitz *et al* 2018). Such a scenario would likely yield synchronous carbon isotope responses or benthic records that lag planktonic $\delta^{13}C$ given the advection time of deep waters in the Atlantic.

Direct comparison of the planktonic and atmospheric $\delta^{13}C$ records indicates that surface ocean $\delta^{13}C$ anomalies during HS1 and the YD were approximately twice as large as those in the atmosphere. Assuming isotopic equilibration between atmospheric CO_2 and surface ocean DIC, we estimate the anticipated $\delta^{13}C_{DIC}$ for the Brazil Margin using available atmospheric $\delta^{13}C$ records and local Mg/Ca-based SST estimates. The resulting curve is broadly similar to our *G. sacculifer* $\delta^{13}C$ results, which suggests that temperature-mediated air-sea gas exchange had an important influence on surface ocean $\delta^{13}C_{DIC}$ in the South Atlantic subtropical gyre. Both *G. sacculifer* and *N. dutertrei* display a larger than predicted $\delta^{13}C$ signal during HS1, however. In the case of *N. dutertrei*, this may reflect transport of isotopically light carbon from the sub-Antarctic where either weakening of the biological pump or upwelling of ^{13}C-depleted water yielded negative carbon isotope anomalies. Alternatively, less air-sea equilibration in the source region for upper thermocline waters could feasibly yield larger than expected *N. dutertrei* anomalies during HS1.

Acknowledgments

We would like to thank two anonymous reviewers whose input greatly improved the manuscript. We are grateful to Lora Wingate and Alexandra Skrivanek for help with stable isotope analyses and to Jim Broda and Ellen Roosen for core collection and curation at the WHOI core lab. Lastly, we would like to acknowledge Bill Curry and Delia Oppo for their foresight in gathering the transect of sediment cores at the Brazil Margin.

ORCID iDs

D Lund https://orcid.org/0000-0002-4847-2889

References

Anand P, Elderfield H and Conte M H 2003 Calibration of Mg/Ca thermometry in planktonic foraminifera from a sediment trap time series *Paleoceanography* **18** 28–1

Arbuszewski J A, Demenocal P B, Cléroux C, Bradtmiller L and Mix A 2013 Meridional shifts of the Atlantic intertropical convergence zone since the last glacial maximum *Nat. Geosci.* **6** 959–62

Barker S, Diz P, Vautravers M J, Pike J, Knorr G, Hall I R and Broecker W S 2009 Inter-hemispheric Atlantic seesaw response during the last deglaciation *Nature* **457** 1097–102

Bauska T K *et al* 2016 Carbon isotopes characterize rapid changes in atmospheric carbon dioxide during the last deglaciation *Proc. Natl Acad. Sci. USA* **113** 3465–70

Boyle E A and Keigwin L D 1985 Comparison of Atlantic and Pacific paleochemical records for the last 215 000 years: changes in deep ocean circulation and chemical inventories *Earth Planet. Sci. Lett.* **76** 135–50

Broecker W S 1982 Ocean chemistry during glacial time *Geochim. Cosmochim. Acta* **46** 1689–705

Carlson A E, Oppo D W, Came R E, LeGrande A N, Keigwin L D and Curry W B 2008 Subtropical Atlantic salinity variability and Atlantic meridional circulation during the last deglaciation *Geology* **36** 991–4

Curry W B and Crowley T J 1987 The $\delta^{13}C$ of equatorial Atlantic surface waters: implications for ice age CO_2 levels *Paleoceanography* **2** 489–517

Curry W B and Oppo D W 2005 Glacial water mass geometry and the distribution of delta C-13 of ΣCO_2 in the western Atlantic ocean *Paleoceanography* **20** PA1017

Fairbanks R G, Sverdlove M, Free R, Wiebe P H and Be A W H 1982 Vertical-distribution and isotopic fractionation of living planktonic-foraminifera from the Panama Basin *Nature* **298** 841–4

Gordon A L 1981 South Atlantic thermocline ventilation *Deep Sea Res.* A **28** 1239–64

Hertzberg J E, Lund D C, Schmittner A and Skrivanek A L 2016 Evidence for a biological pump driver of atmospheric CO_2 rise during Heinrich stadial 1 *Geophys. Res. Lett.* **43** 12242–51

Hoffman J L and Lund D C 2012 Refining the stable isotope budget for Antarctic bottom water: new foraminiferal data from the abyssal southwest Atlantic *Paleoceanography* **27** PA1213

Kroopnick P M 1985 The distribution of $\delta^{13}C$ of ΣCO_2 in the world oceans *Deep Sea Res.* A **32** 57–84

Lacerra M, Lund D, Yu J and Schmittner A 2017 Carbon storage in the mid-depth Atlantic during millennial-scale climate events *Paleoceanography* **32** 780–95

Lamy F, Kaiser J, Arz H W, Hebbeln D, Ninnemann U, Timm O, Timmermann A and Toggweiler J R 2007 Modulation of the bipolar seesaw in the southeast pacific during termination 1 *Earth Planet. Sci. Lett.* **259** 400–13

Locarnini R A *et al* 2013 *World Ocean Atlas 2013, Volume 1: Temperature* ed S Levitus and A Mishonov 74th edn (NOAA Atlas NESDIS) (https://data.nodc.noaa.gov/woa/WOA13/DOC/woa13_vol1.pdf)

Lund D C, Tessin A C, Hoffman J L and Schmittner A 2015 Southwest Atlantic water mass evolution during the last deglaciation *Paleoceanography* **30** 477–94

Lynch-Stieglitz J, Valley S G and Schmidt M W 2019 Temperature-dependent ocean-atmosphere equilibration of carbon isotopes in surface and intermediate waters over the deglaciation *Earth Planet. Sci. Lett.* **506** 466–75

Martínez-García A *et al* 2014 Iron fertilization of the sub-Antarctic ocean during the last Ice Age *Science* **343** 1347–50

Menviel L *et al* 2018 Southern Hemisphere westerlies as a driver of the early deglacial atmospheric CO_2 rise *Nat. Commun.* **9** 2503

Menviel L, Mouchet A, Meisnner K J, Joos F and England M H 2015 Impact of oceanic circulation changes on atmospheric $\delta^{13}CO_2$ *Glob. Biogeochem. Cycles* **29** 1944–61

Monnin E, Indermühle A, Dällenbach A, Flückiger J, Stauffer B, Stocker T F, Raynaud D and Barnola J M 2001 Atmospheric CO_2 concentrations over the last glacial termination *Science* **291** 112–4

Mulitza S *et al* 1999 The South Atlantic carbon isotope record of planktonic foraminifera *Use of Proxies in Paleocanography: Examples from the South Atlantic* ed G Fischer and G Wefer (Berlin: Springer) pp 427–45

Neftel A, Oeschger H, Schwander J, Stauffer B and Zumbrunn R 1982 Ice core sample measurements give atmospheric CO_2 content during the past 400 00 yr *Nature* **295** 220–3

Ninnemann U S and Charles C D 1997 Regional differences in quaternary sub Antarctic nutrient cycling: Link to intermediate and deep water ventilation *Paleoceanography* **12** 560–67

Oppo D W, Curry W B and McManus J F 2015 What do benthic d13C and d18O data tell us about Atlantic circulation during Heinrich stadial 1? *Paleoceanography* **30** 353–68

Pahnke K, Zahn R, Elderfield H and Schulz M 2003 340 000-year centennial-scale marine record of southern hemisphere climatic oscillation *Science* **301** 948–52

Parrenin F *et al* 2013 Synchronous change of atmospheric CO_2 and Antarctic temperature during the last deglacial warming *Science* **339** 1060–3

Peterson R G and Stramma L 1991 Upper-level circulation in the south Atlantic ocean *Prog. Oceanogr.* **26** 1–73

Provost C, Escoffier C, Maamaatuaiahutapu K, Kartavtseff A and Garçon V 1999 Subtropical mode waters in the south Atlantic ocean *J. Geophys. Res.: Oceans* **104** 21033–49

Rosenthal Y, Boyle E A and Slowey N 1997 Temperature control on the incorporation of magnesium, strontium, fluorine, and cadmium into benthic foraminiferal shells from Little Bahama bank: prospects for thermocline paleoceanography *Geochim. Cosmochim. Acta* **61** 3633–43

Schmitt J *et al* 2012 Carbon isotope constraints on the deglacial CO_2 rise from ice cores *Science* **336** 711–4

Schmittner A and Lund D C 2015 Early deglacial Atlantic overturning decline and its role in atmospheric CO_2 rise inferred from carbon isotopes *Clim. Past* **11** 135–52

Sigman D M, Hain M P and Haug G H 2010 The polar ocean and glacial cycles in atmospheric CO_2 concentration *Nature* **466** 47–55

Spero H J, Bijma J, Lea D W and Bemis B E 1997 Effect of seawater carbonate concentration on foraminiferal carbon and oxygen isotopes *Nature* **390** 497–500

Spero H J and Lea D W 1993 Intraspecific stable-isotope variability in the planktic foraminifera globigerinoides sacculifer—results from laboratory experiments *Mar. Micropaleontol.* **22** 221–34

Spero H J and Lea D W 1996 Experimental determination of stable isotope variability in globigerina bulloides: implications for paleoceanographic reconstructions *Mar. Micropaleontol.* **28** 231–46

Spero H J and Lea D W 2002 The cause of carbon isotope minimum events on glacial terminations *Science* **296** 522–5

Spero H J, Mielke K M, Kalve E M, Lea D W and Pak D K 2003 Multispecies approach to reconstructing eastern equatorial pacific thermocline hydrography during the past 360 kyr *Paleoceanography* **18** 16

Stramma L and England M 1999 On the water masses and mean circulation of the south Atlantic ocean *J. Geophys. Res.: Oceans* **104** 20863–83

Stramma L, Ikeda Y and Peterson R G 1990 Geostrophic transport in the Brazil current region north of 20°S *Deep Sea Res.* A **37** 1875–86

Tessin A C and Lund D C 2013 Isotopically depleted carbon in the mid-depth South Atlantic during the last deglaciation *Paleoceanography* **28** 296–306

Tomczak M and Godfrey J S 1994 *Regional Oceanography: An Introduction* (Oxford: Pergammon) (https://doi.org/10.1002/joc.3370150511)

Tsuchiya M, Talley L D and McCartney M S 1994 Water-mass distributions in the western south Atlantic; a section from south Georgia island (54S) northward across the equator *J. Mar. Res.* **52** 55–81

Veres D *et al* 2012 The Antarctic ice core chronology (AICC2012): an optimized multi-parameter and multi-site dating approach for the last 120 thousand years *Clim. Past Discuss.* **8** 6011–49

Zeebe R E, Bijma J and Wolf-Gladrow D A 1999 A diffusion-reaction model of carbon isotope fractionation in foraminifera *Mar. Chem.* **64** 199–227

Zhang J *et al* 2017 Asynchronous warming and oxygen isotope evolution of deep Atlantic water masses during the last deglaciation *Proc. Natl Acad. Sci. USA* **114** 11075–80

Zhang J, Quay P D and Wilbur D O 1995 Carbon isotope fractionation during gas-water exchange and dissolution of CO_2 *Geochim. Cosmochim. Acta* **59** 107–14